Thermodynamic Characterization of Nucleoplasmin Unfolding: Interplay between Function and Stability[†]

Guillermo Franco, Sonia Bañuelos, Jorge Falces, Arturo Muga, and María A. Urbaneja*

Unidad de Biofísica (CSIC-UPV/EHU) and Departamento de Bioquímica y Biología Molecular, Universidad del País Vasco, Apdo 644, 48080 Bilbao, Spain

Received February 13, 2008; Revised Manuscript Received May 27, 2008

ABSTRACT: The unfolding equilibrium of recombinant (rNP) and natural variants of nucleoplasmin (NP) from *Xenopus laevis* has been analyzed using biochemical and spectroscopic techniques. In the presence of denaturing concentrations of guanidinium salts (GuHCl and GuSCN), both domains, core and tail, of the rNP pentamer unfold as proven using single-carrying tryptophan mutants, whereas urea is remarkably unable to fully unfold rNP. Chemical unfolding is reversible and can be described well as a two-state transition in which the folded pentamer is directly converted to unfolded monomers, with no evidence of (partially) folded monomers. Therefore, rNP dissociates and fully unfolds simultaneously ($N_5 \leftrightarrow 5U$). Activation of the protein by hyperphosphorylation is accompanied by a destabilization of the protein oligomer. A comparison of natural NP forms isolated from eggs and oocytes of *X. laevis* and recombinant NP reveals that natural variants can be fully unfolded by urea and exhibit D_{50} (denaturant concentration at the transition midpoint) values lower than that of the nonphosphorylated protein. Progressive phosphorylation of NP correlates with a gradual loss of stability of 6 kcal/mol (oNP) and 10 kcal/mol (eNP), as compared with the nonphosphorylated protein pentamer. These results suggest that the remarkable stability of the recombinant protein is required to cope with the destabilization brought about by its phosphorylation-induced activation.

Nucleoplasmin (NP),[1] primarily isolated from either eggs or oocytes of *Xenopus laevis*, is a protein that has an active role in chromatin assembly and remodeling (*1–4*). Nucleoplasmin is acidic and thermostable and assembles into pentamers. Each monomer is 200 amino acid residues long and consists of two domains, namely, the core, corresponding to the 120 N-terminal residues, and the C-terminal tail. The core domain is responsible for NP oligomerization and folds into an eight-stranded β-barrel with a "jellyroll" topology (*5, 6*). A continuous ring of conserved apolar residues within the pentamer seems to play an essential role in conferring thermostability (*5*). The tail domain contains a region rich in negatively charged residues (20 Asp and Glu residues among residues 120−150), termed "poly-Glu" or acidic tract 2 (A2), and a nuclear localization signal (NLS) belonging to the bipartite class. Spectroscopic and predictive methods have indicated that this domain adopts a natively disordered conformation (*7*), which may modulate the interaction of the protein with diverse ligands (*8*).

The activity of NP is modulated by phosphorylation at multiple residues (*10*). NP isolated from both *X. laevis* oocytes (oNP) and eggs (eNP), corresponding to a later stage of maturation, contain an increasing number of phosphoryl moieties per monomer (*7*), and the location of eight of them has recently been determined by mass spectrometry (*10*). At the oocyte stage, NP is already active in histone binding, while the higher degree of phosphorylation of egg NP correlates with a higher sperm decondensation activity, reflecting the fact that during the maturation of eggs NP acquires an optimal activity for subsequent fertilization (*2*).

Posttranslational modification by phosphorylation is a ubiquitous regulatory mechanism in both eukaryotes and prokaryotes which provides the cell with a tool for modulating many diverse processes. There seems to be no universal mechanism by which phosphorylation modulates protein function, although it has been observed that repulsive electrostatic effects dominate the response of proteins to phosphorylation in a number of systems (*11*).

In this work, we characterize the conformational stability of this pentameric protein by equilibrium unfolding studies, using urea and guanidinium salts as protein denaturants. Analysis of the unfolding curves provides a measure of the conformational stability of the phosphorylated, natural protein variants and the nonphosphorylated, recombinant protein. Our data show that pentameric NP dissociates and unfolds in a concomitant process and that progressive phosphorylation during egg maturation results in significant protein destabi-

[†] This work was supported by the Ministerio de Educación y Ciencia (Grant BFU2004-03452/BMC), the Universidad del País Vasco (Grants UPV13505 and GIU06/48), and Diputación Foral de Bizkaia (Grant DIPE06/20). G.F. held a predoctoral fellowship from the Gobierno Vasco. J.F. holds a predoctoral fellowship from the Universidad del País Vasco, and S.B. is supported by a Ramón y Cajal contract.

* To whom correspondence should be addressed. Telephone: +34-94-601-3352. Fax: +34-94-601-3360. E-mail: gbpurarm@lg.ehu.es.

[1] Abbreviations: eNP, nucleoplasmin isolated from eggs of *X. laevis*; NP, nucleoplasmin; oNP, nucleoplasmin purified from oocytes of *X. laevis*; rNP, recombinant nucleoplasmin overexpressed in *Escherichia coli*; rNPW19F, recombinant mutant with residue 19 mutated to phenylalanine; rNPW126F, recombinant mutant with residue 126 mutated to phenylalanine; GuHCl, guanidine hydrochloride; GuSCN, guanidine thiocyanate; N_5, nucleoplasmin (folded) pentamer; 5U, five unfolded nucleoplasmin monomers.

10.1021/bi8002555 CCC: $40.75
Published on Web 07/03/2008

lization. This finding suggests that the remarkable chemical and thermal stability of nonphosphorylated rNP might be necessary for the protein to cope with the phosphorylation-induced destabilization, which in turn is required for protein activation.

EXPERIMENTAL PROCEDURES

Chemicals. All chemicals were purchased from Sigma. Chemical denaturants urea, guanidine hydrochloride (GuHCl), and guanidine thiocyanate (GuSCN) were of the highest purity.

Cloning of Single-Tryptophan Mutant NPs. Mutants rNPW19F and rNPW126F were obtained by PCR-based site-directed mutagenesis using wild-type NP cloned in pET11b (*7, 12*) as a template: codons 19 and 126 were substituted, respectively, in a three-step mutation cycle for TTC, encoding Phe. The sequence of the mutants was checked by DNA sequencing. *Escherichia coli* BL21(DE3) cells were transformed with the resultant plasmids.

Proteins. Recombinat wild-type and single-tryptophan mutant NPs as well as natural NP from *X. laevis* oocytes and eggs were purified as described previously (*7*). The concentration of nucleoplasmin was determined using the bicinchoninic acid system (Pierce, Rockford, IL). Expression of protein concentration throughout the text always corresponds to pentameric NP.

Fluorescence Experiments. The NP unfolding reactions were performed in 50 mM phosphate buffer (pH 6.5) containing varying concentrations of denaturants (0−10 M for urea, 0−8 M for GuHCl, and 0−3 M for GuSCN). The protein concentration was 0.011−1.1 mg/mL for rNP and 0.11−0.22 mg/mL for oNP and eNP. Spectroscopic measurements were performed upon incubation of the protein for 3 h with GuSCN and 12 h with GuHCl and urea at 25 °C. Longer incubation times gave identical results.

Samples were excited at 280, and their fluorescence-corrected emission spectra were recorded between 290 and 450 nm in an SLM-8100 spectrofluorimeter (Aminco) at 25 °C, using 0.3 cm × 0.3 cm cuvettes and slit widths of 4 nm. Spectra were corrected for the solvent signal and inner filter effect. In fluorescence anisotropy measurements, emission depolarization was assessed at 330 nm upon excitation at 280 nm. Quenching experiments were performed adding increasing concentrations of acrylamide to 1 μM native or 2.5 M GuSCN-treated rNP, under the same experimental conditions.

Circular Dichroism (CD) Spectroscopy. Far-UV CD spectra were recorded between 250 and 190 nm in a Jasco J-810 spectropolarimeter at 25 °C. Each spectrum is the average of four scans measured taking a data point every 0.2 nm with a 2 s integration time and a 1 nm bandwidth. The protein concentration was 0.5 mg/mL, and the path length of the quartz cell was 0.01 cm. All spectra were corrected by subtracting the baseline of the buffer solution [50 mM Tris-HCl (pH 6.5)], recorded under the same conditions. Mean ellipticity values were calculated using the expression $\theta = \varepsilon/10cnl$, where ε is the ellipticity (millidegrees), c is the protein concentration (moles per liter), l is the cuvette path length, and n is the number of amino acid residues in the protein (200).

Gel-Filtration Chromatography. NP samples (60 μM, 25 μL) were loaded onto a calibrated Superdex 200 HR 10/30 gel-filtration column (GE Healthcare). Equilibration and elution were performed with 50 mM phosphate buffer (pH 6.5) containing the desired denaturant concentration at a flow rate of 0.5 mL/min at room temperature. A_{280} was recorded. The column was calibrated in the absence and presence of denaturants with the appropriate standards (gel filtration standards, Bio-Rad).

Analytical Ultracentrifugation Analysis. (a) Sedimentation Velocity Analysis. Protein samples (0.5 mg/mL) in 50 mM PBS buffer and with different GdnCl concentrations (0−7.15 M) were loaded on an An50Ti rotor. Long column (400 μL) sedimentation velocity experiments were performed at 50000 rpm and 20 °C in an XL-A analytical ultracentrifuge (Beckman-Coulter) using double-sector Epon-charcoal centerpieces. Absorbance scans (0.005 cm step size) were taken at 280 nm. Differential sedimentation coefficient distributions, $c(s)$, were calculated by least-squares boundary modeling of sedimentation velocity data using SEDFIT (*13, 14*). From this analysis, the obtained sedimentation coefficient were corrected for solvent composition and temperature with SEDNTERP to yield $s_{20,w}$.

(b) Sedimentation Equilibrium Analysis. Short column (75 μL) sedimentation equilibrium experiments with the same samples were performed. Absorbance scans at equilibrium were carried out at 11000, 19000, and 22000 rpm, and the measurement was conducted at the appropriate wavelength. Baseline offsets were measured afterward at 50000 rpm. Whole-cell weight-average buoyant molar masses (bM_w) were obtained by fitting the experimental data to the equation for the radial concentration distribution of an ideal solute at sedimentation equilibrium, using EQASSOC (supplied by Beckman-Coulter) (*15*). The corresponding apparent weight-average molar masses ($\bar{M}_{w,a}$) were determined from the buoyant masses taking into account the partial specific volumes of the protein calculated from the amino acid composition with SEDNTERP (*16*). In the presence of denaturants, the apparent partial specific volume of the protein can be calculated according to the method of ref *17*.

Native Polyacrylamide Gel Electrophoresis (PAGE). Native NP and denaturant-treated NP were analyzed by native PAGE (PHAST system, Amersham), using 8−25% acrylamide gels. Samples were run at 245 AVH and 15 °C. The gels were stained with Coomassie blue.

Equilibrium Data Analyses. rNP unfolding was described as a two-state transition with the native pentamer directly converted to denatured monomers ($N_5 \leftrightarrow 5U$).

The equilibrium constant of the unfolding reaction, K_u, and the free energy of unfolding, ΔG_u, are defined as

$$K_u = [U]^5/[N_5] = 5Pt^4 f_u^5/(1 - f_u) \quad (1)$$

$$\Delta G_u = -RT \ln K_u \quad (2)$$

where Pt is the total protein monomer concentration and f_u the fraction of denatured protein. At any given denaturant concentration [D], f_u was calculated as the ratio

$$f_u = \frac{I - I_n}{I_u - I_n} \quad (3)$$

where I is the fluorescence value at a given denaturant concentration and I_n and I_u are the fluorescence values

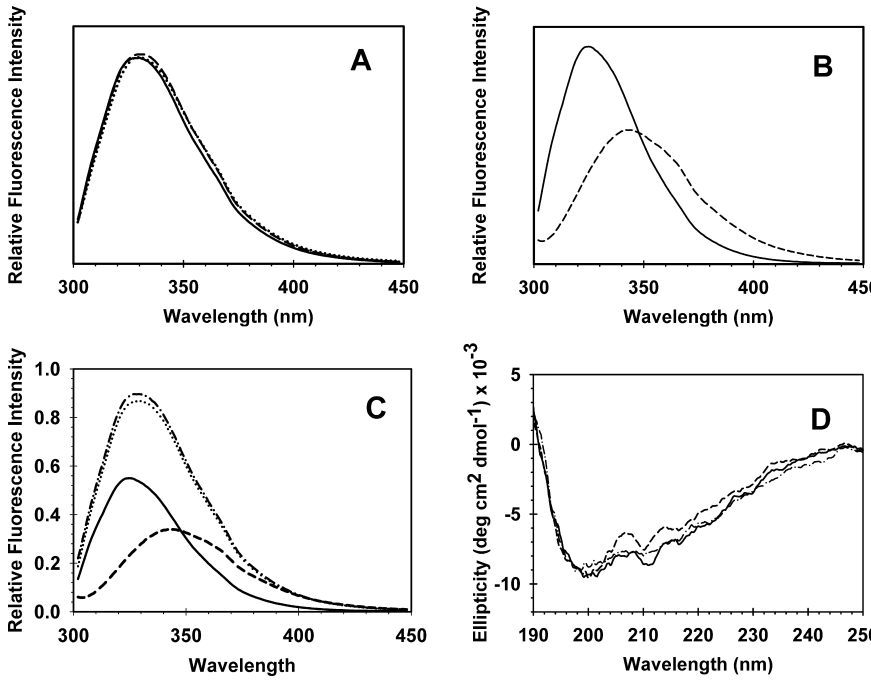

FIGURE 1: Fluorescence emission properties of nucleoplasmin. (A) Emission fluorescence spectra of recombinant (solid line), oocyte (dotted line), and egg nucleoplasmin (dashed line) in 50 mM phosphate buffer (pH 6.5) at 25 °C. The spectra were corrected for the buffers. The excitation wavelength was 280 nm, with excitation and emission slits of 4 nm each and a scan rate of 60 nm/min. (B) Emission fluorescence spectra of recombinant single-tryptophan mutants: rNPW126F (solid line) and rNPW19F (dashed line). (C) Decomposition of the recombinant NP overall emission spectrum into two emitting components (solid and dashed lines). The addition of both components (dotted−dashed line) superimposes on the experimental emission spectrum (dotted line). (D) UV CD spectra of recombinant wild-type rNP (solid line), rNPW19F (dashed line), and rNPW126F (dashed−dotted line).

corresponding to the native (n) and denatured (u) states of the protein, respectively. To calculate m and $\Delta G_u^{H_2O}$, the ΔG_u values obtained for denaturant concentrations within the transition zone of the unfolding curve were used to fit the equation

$$\Delta G_u = \Delta G_u^{H_2O} - m[D] \quad (4)$$

RESULTS

The stability of recombinant and natural NPs has been studied following the effect of urea, guanidinium chloride, and guanidinium thiocyanate on the spectroscopic and biochemical properties of these protein variants. Due to the availability of larger quantities of rNP, as compared to natural NPs, and to its higher homogeneity (rNP is not phosphorylated), unfolding of rNP is used as a model for the natural variants. The comparison of the three protein variants provides information about the effect of phosphorylation on NP stability (see below).

The overall emission spectra of the three NPs, with maxima ranging from 330 to 332 nm, show a rather broad and asymmetric band (Figure 1A) that might reflect a different contribution of the two tryptophan residues (W19 and W126) to the global fluorescence of the protein (*18*). The use of single-point mutants in which one of these residues is replaced with phenylalanine indicates that this is the case. These mutations do not significantly modify protein conformation as judged from their stability and far-UV CD spectra (Figure 1D), which resemble those of wild-type rNP. The emission maxima of rNPW19F and rNPW126F are centered at 341 and 325 nm, respectively, the fluorescence intensity of the former being approximately half of that observed for rNPW126F (Figure 1B). The overall fluorescence spectra of NP can be properly fitted with two components, one arising mainly from W19, located in the hydrophobic core region of the protein (*5*), and contributing to the global fluorescence twice as much as W126, located in the hydrophilic tail domain (Figure 1C).

Effect of Denaturants on Nucleoplasmin Unfolding. The fluorescence emission spectra of native and fully denatured rNP excited at 280 nm are shown in Figure 2A. While native rNP has an emission maximum near 330 nm, in the presence of 2.5 M GuSCN its emission maximum shifts to 346 nm with a concomitant decrease in emission intensity. Both effects are usually attributed to an increased level of solvent exposure of previously buried indole rings upon protein unfolding (*19*). Unfolding equilibrium curves are obtained by plotting the fluorescence emission intensity at 331 nm as a function of denaturant concentration (Figure 2B). Similar profiles are observed for maximum emission wavelength, the ratio of fluorescence intensity I_{355}/I_{320}, and the steady-state anisotropy of the protein. The denaturant-induced decrease in anisotropy suggests that protein unfolding is accompanied by dissociation of its oligomeric structure. The plot of the full width at half-height (fwhh) value of the overall emission band as a function of GuSCN concentration shows a peak at a denaturant concentration that corresponds to D_{50} values [denaturant concentration at the transition midpoint (Figure 2B, inset, and Table 1)]. fwhh reflects the heterogeneity of the signal coming from the two tryptophan residues of rNP: the broader the emission band, the more heterogeneous the chemical environment of the fluorophores, as expected for the transition state. Fluorescence quenching studies of rNP in the absence and presence of denaturing GuSCN concentrations further prove that rNP is unfolded above 2.5 M

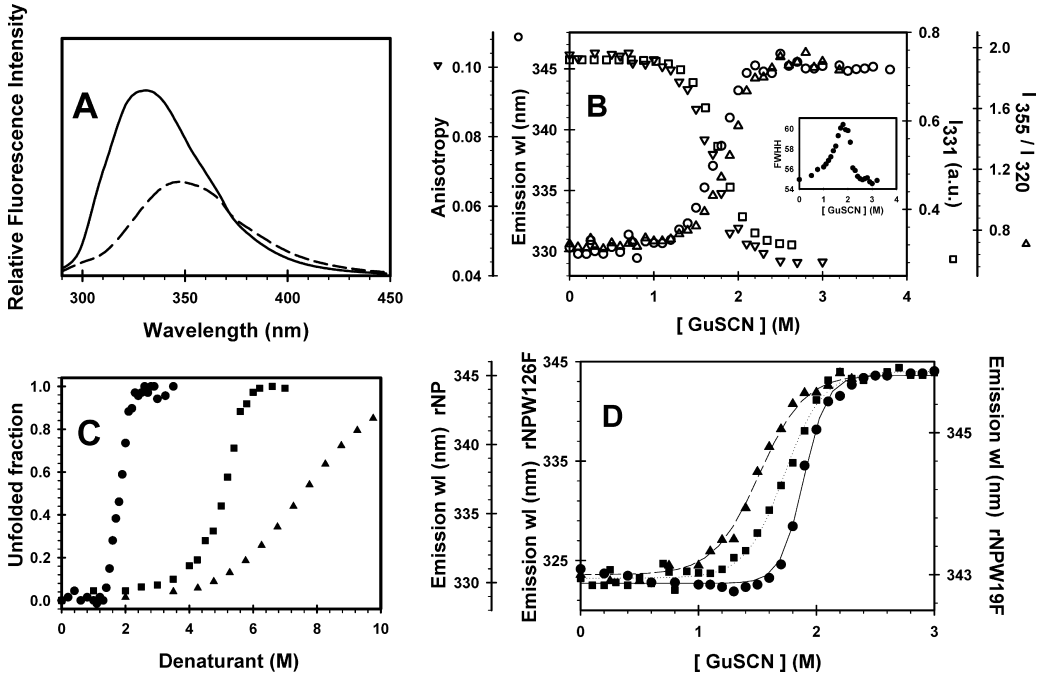

FIGURE 2: Effect of denaturants on the fluorescence emission properties of recombinant nucleoplasmin. (A) Emission spectra of native (solid line) and GuSCN-denatured (dashed line) rNP. (B) Fluorescence properties of rNP as a function of GuSCN concentration: (○) maximum emission wavelength, (□) emission intensity at 331 nm, (△) emission intensity ratio at 355 and 320 nm, and (▽) anisotropy. The inset shows the GuSCN concentration dependence of the full width at half-height. (C) Fraction of unfolded rNP as a function of denaturant concentration: (●) GuSCN, (■) GuHCl and (▲) urea. (D) Maximum fluorescence emission wavelength of (●) rNPW126F, (▲) rNPW19F, and (■) rNP as a function of GuSCN concentration. Their corresponding fittings are included (solid line for rNPW126F, dotted line for rNP, and dashed line for rNPW19F).

Table 1: Best Fit Parameters for the Unfolding of rNP[a] by GuSCN[b,c]

fluorescence parameter	D_{50} (M)	m[d] (kcal mol^{-1} M^{-1})	$\Delta G_{unf,w}$ (kcal/mol)[d]
I_{331}	1.78 ± 0.12	−11.8 ± 1.3	48.9 ± 2.7
λ_{max}	1.78 ± 0.15	−11.6 ± 1.6	48.2 ± 1.8
anisotropy	1.76 ± 0.06	−10.6 ± 2.2	46.6 ± 3.5
I_{355}/I_{325}	1.86 ± 0.13	−11.2 ± 0.9	49.1 ± 3.0

[a] The rNP concentration was 2 μM. [b] Abbreviations: D_{50}, denaturant concentration at the transition midpoint; m, dependence of ΔG_{unf} on denaturant concentration; $\Delta G_{unf,w}$, free energy extrapolated to zero denaturant concentration. [c] The $\Delta G°$ of multimeric proteins has a non-zero value at D_{50}, when denatured fraction $f_D = 0.5$ (*21*). [d] $\Delta G_{unf,w}$ calculated using a 5-mer to 1-mer reaction mechanism as described in Experimental Procedures. Values are average results of at least three experiments.

GuSCN, since the Stern−Volmer constant (K_{sv}) that denotes the accessibility of tryptophan residues to acrylamide increases from 4.53 M^{-1} for native rNP to 8.27 M^{-1} for the denatured protein, in agreement with the K_{sv} value reported for other unfolded proteins (*20*).

The highest attainable urea concentration (9.8 M) is not able to fully unfold this remarkably stable pentameric protein, revealing itself as the least effective denaturant in inducing rNP unfolding (Figure 2C). In contrast, guanidinium salts completely unfold rNP as judged by the denaturant-induced changes in the fluorescence parameters mentioned above (Figure 2B,C). The D_{50} value for GuSCN is 1.78 M, while that for GuHCl is 3-fold higher (5.1 M). The unfolding process is completely reversible, as assessed by the fluorescence properties of a sample unfolded in 2.5 M GuSCN and extensively dialyzed to remove the denaturant, which are found to be identical to those of native rNP (not shown). When rNPW126F and rNPW19F are denatured, their respective emission λ_{max} values shift to 345−346 nm as well (Figure 2D). Single-tryptophan mutants present a cooperative unfolding process with slightly different D_{50} values [1.54 and 1.92 M for rNPW19F and rNPW126F, respectively (Figure 2D)] compared to that of rNP (1.78 M). The analysis of the unfolding curves using a two-state model (see below) allows us to estimate the thermodynamic parameters of the unfolding process (shown for rNP in Table 1).

To further clarify the unfolding pathway of rNP in the presence of GuSCN, protein samples containing different concentrations of denaturing agent were subjected to native PAGE and size exclusion chromatography under quasi-equilibrium conditions (Figure 3A,B). Two different species are mainly detected during the unfolding transition of NP, one corresponding to the pentameric protein which coexists with a second band tentatively assigned to monomeric rNP in the 1.2−2 M GuSCN concentration range and completely disappears at 2.5 M GuSCN. Regardless of the denaturant concentration, only the bands corresponding to the monomeric or pentameric species are observed, without evidence of intermediate oligomerization states (Figure 3A). Size exclusion chromatography shows that dissociation of pentameric rNP into monomers starts above 1.2 M GuSCN. The calculated mass for these monomers was 22 kDa, according to the calibration of the size exclusion column under denaturing conditions. A further increase in the GuSCN concentration induced a progressive increase in the monomeric fraction that becomes the most abundant species at >2 M denaturant. It is noteworthy that the elution volume of the pentameric protein shows a gradual shift to lower values with an increase in denaturant concentration, suggesting that its hydrodynamic properties change prior to unfolding, most likely due to an expansion of the native pentamer. This effect, also seen during native PAGE, might

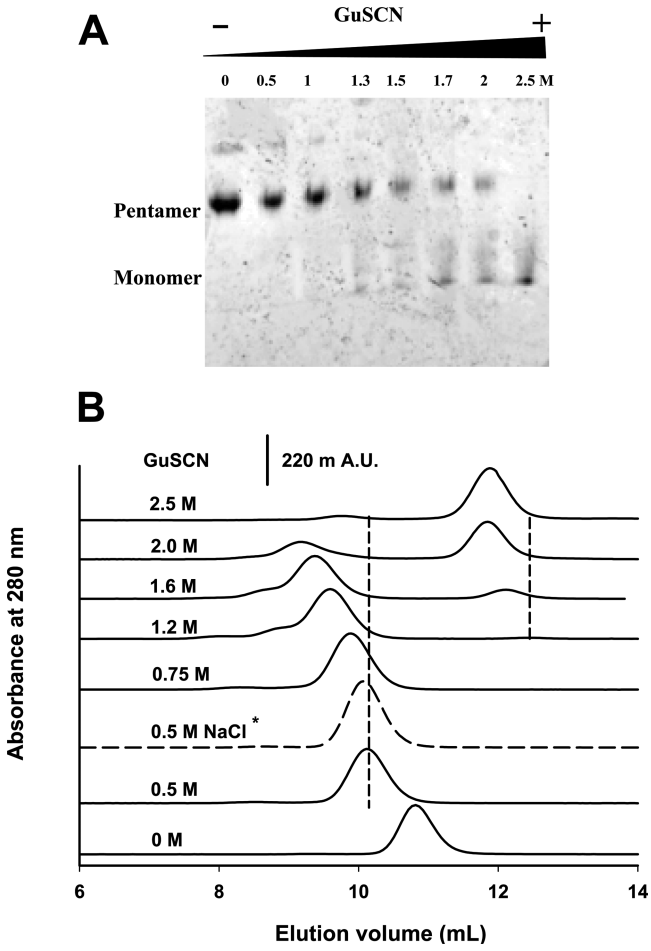

FIGURE 3: Oligomeric state of rNP during the unfolding transition. (A) rNP oligomeric state determined from its mobility in native polyacrylamide gels. Protein samples previously incubated with increasing GuSCN concentrations were run and stained with Coomassie blue. The different species are indicated at the left. (B) Size exclusion chromatography of rNP incubated with increasing concentrations of GuSCN. The experiments were carried out as described in Experimental Procedures.

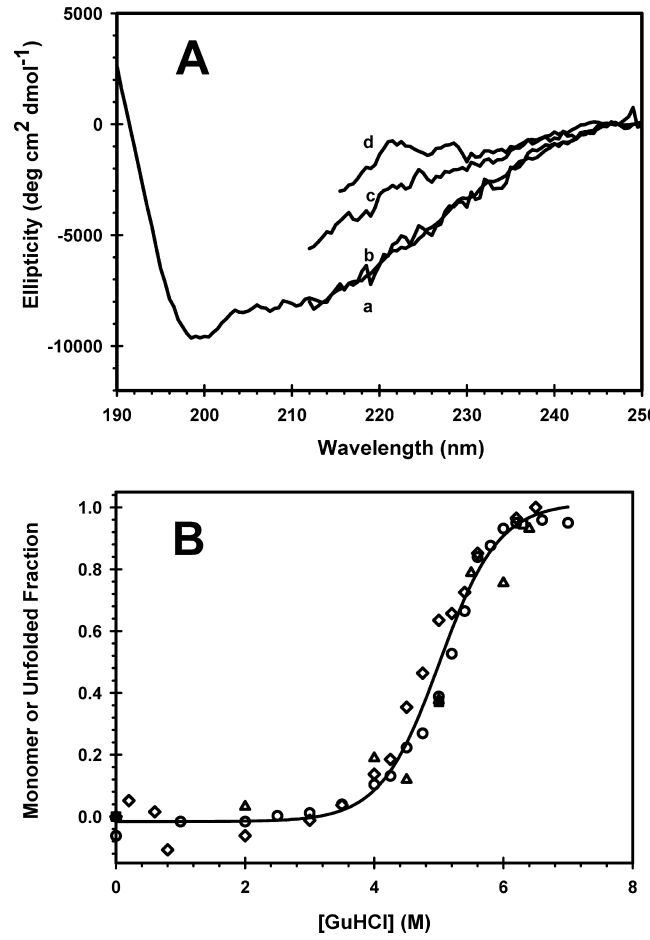

FIGURE 4: GuHCl-induced unfolding of rNP. (A) Samples of rNP were incubated with different concentrations of GuHCl (0−7.5 M) in buffer and monitored by CD. Mean of four spectra of rNP in the presence of 0 (curve a), 3 (curve b), 5 (curve c) and 6.5 M GuHCl (curve d) acquired at 25 °C after overnight incubation. Absorption of GuHCl in the far-UV region precluded registering the spectra beyond 210 nm. (B) Unfolding transition of rNP with GuHCl monitored by different methods. Samples of rNP were incubated with different concentrations of GuHCl (0−7.5 M) in buffer. Dissociation and unfolding were monitored by different biochemical and biophysical methods. The fraction of monomer or unfolded protein as a function of denaturant concentration was calculated on the basis of the fluorescence (○), circular dichroism (◇), native polyacrylamide gel electrophoresis (△), and gel filtration (□) results. The solid line represents the global fitting of all data obtained by different techniques.

come from electrostatic interactions with GuSCN, since addition of 0.5 M NaCl to rNP induces a shift similar to that observed in the presence of the same denaturant concentration (Figure 3B). The emission fluorescence spectrum of the protein chromatographically processed upon addition of NaCl corresponds to a folded protein. The pentameric and monomeric fractions eluted from the column at 1.6 M denaturant show emission wavelengths characteristic of folded and unfolded NP, respectively, when measured immediately after elution, thus supporting the hypothesis that oligomer dissociation and monomer unfolding are tightly coupled reactions.

We also characterized the native and unfolded states of nucleoplasmin by analytical centrifugation. Velocity sedimentation experiments with native rNP render a unique molecular population with an $s_{20,w}$ of 5.2 ± 0.5 S, compatible with a pentamer, in agreement with the mean molecular mass obtained by sedimentation equilibrium, 103700 ± 5000 Da (oligomerization state $N = 4.7 \pm 0.3$) (*22*). Because of technical limitations in using GuSCN with the ultracentrifuge cuvettes, rNP was incubated with GuHCl at a denaturing concentration (7 M). The result, an $s_{20,w}$ of 1.5 S and a molecular mass of 31000 Da ($N = 1.2$), is compatible with denaturant-induced pentamer dissociation. The sedimentation coefficient is lower than expected for a globular monomer ($s_{20,w} = 2.3$ S), suggesting that the monomer is unfolded. This is further demonstrated by the loss of secondary structure during the unfolding transition detected by CD spectroscopy (Figure 4A). As previously reported (*7, 12*), the far-UV CD spectrum of rNP exhibited two minima at 198 and 213 nm that indicate the presence of nonregular and β-structure conformations, respectively. The decrease in the ellipticity value at 222 nm with an increase in denaturant concentration indicates protein unfolding, which can be better characterized by estimating f_N and f_U from the fractional change in ellipticity at 222 nm versus GuHCl concentration (Figure 4B).

The experimental transitions monitored with different techniques are properly fitted using a two-state model, in which pentamer dissociation and monomer denaturation are

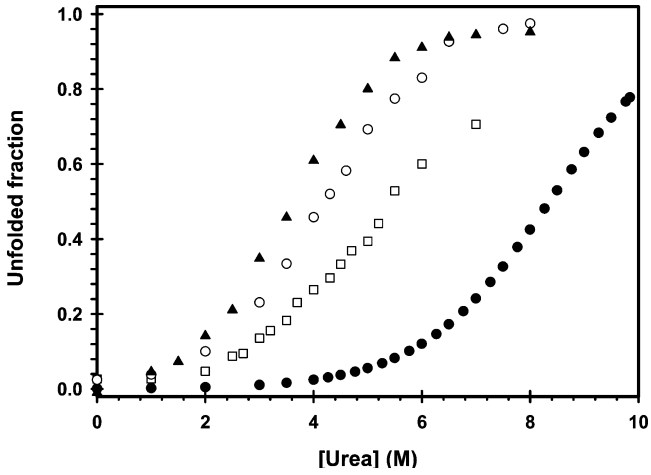

FIGURE 5: Nucleoplasmin stability against urea depends on the phosphorylation level of the protein. Samples of rNP (●), oNP (○), and eNP (▲) were incubated with increasing urea concentrations (0−10 M) and their fluorescence properties analyzed as described in Experimental Procedures. The effect of ionic strength (0.15 M NaCl) on eNP stability is also shown (□).

tightly coupled ($N_5 \leftrightarrow 5U$). Indeed, the monomer/pentamer fraction obtained from native PAGE and size exclusion chromatography with increasing GuHCl concentrations perfectly correlates with the two-state unfolding process described by fluorescence spectroscopy (Figure 4B). The good correlation among fluorescence spectroscopy, native gel electrophoresis, gel filtration chromatography, circular dichroism, and analytical ultracentrifugation data indicates that nucleoplasmin is a pentameric protein that simultaneously loses its quaternary, tertiary, and regular secondary structure during the unfolding transition induced by guanidinium salts.

Effect of Phosphorylation on the Stability of the Protein. Natural variants of NP isolated from *Xenopus* oocytes (oNP) and eggs (eNP) contain on average three and seven to ten phosphorylated residues per protein monomer, respectively (*7*), that play an essential role in the biological activation of the protein (*9, 10*). In an attempt to establish a structure−function relationship, we previously found that the secondary structure of the protein was not significantly sensitive to phosphorylation (*7*). Here we compare the stability of nonphosphorylated rNP and of the natural protein variants to explore the putative effect of this posttranslational modification on the tertiary and/or quaternary structure of the protein.

Compared with rNP, the phosphorylated forms of the protein are more sensitive to denaturants (Figure 5). Accordingly, both natural variants (oNP and eNP) are more sensitive to guanidinium salts than nonphosphorylated recombinant rNP (Table 2). In contrast to what was observed for rNP, both oNP and eNP are completely unfolded at 8 M urea, and protein denaturation occurs at lower urea concentrations as the phosphorylation level of the protein increases (rNP < oNP < eNP), showing a steady reduction in the D_{50} and ΔG values as the number of phosphoryl groups increases (Figure 5 and Table 2). An increase in the ionic strength of the buffer (0.15 M NaCl) partially reverts eNP destabilization, as previously observed for oNP (*12*). Table 2 shows the unfolding parameters calculated for rNP and the natural variants (oNP and eNP) in the presence of both guanidinium salts and urea. To estimate the unfolding parameters of rNP, we have assumed that if rNP were fully unfolded by urea, the emission wavelength of its denatured state would be the same as those of oNP and eNP.

Table 2: Thermodynamic Parameters of Different NP Forms[a]

	chaotropic agent	D_{50} (M)	m (kcal mol^{-1} M^{-1})	$\Delta G_{unf,w}$ (kcal/mol)
rNP	GuSCN	1.80 ± 0.04	−11.3 ± 0.5	48.2 ± 1.1
	GuHCl	5.10 ± 0.04	−4.5 ± 0.3	51.1 ± 2.3
	urea[b]	8.35 ± 0.05	−1.8 ± 0.2	45.0 ± 0.9
oNP	GuSCN	1.42 ± 0.04	−12.5 ± 0.1	48.2 ± 0.6
	GuHCl	4.45 ± 0.06	−4.7 ± 0.1	48.9 ± 0.4
	urea	4.15 ± 0.15	−1.9 ± 0.1	38.6 ± 0.7
eNP	GuSCN	1.45 ± 0.05	−9.9 ± 0.1	44.7 ± 1.1
	GuHCl	4.61 ± 0.08	−4.5 ± 0.1	45.2 ± 0.9
	urea	3.52 ± 0.07	−1.8 ± 0.1	34.9 ± 0.3

[a] Abbreviations: D_{50}, denaturant concentration at the transition midpoint; m, dependence of ΔG_{unf} on denaturant concentration; $\Delta G_{unf,w}$, free energy extrapolated to zero denaturant concentration. The following denaturants were used: GuSCN, GuHCl, and urea. Values are average results of at least three experiments. [b] To estimate rNP unfolding parameters, we assume that if urea would fully unfold rNP, the emission wavelength of its denatured state would be the same as those of oNP and eNP.

In spite of the loss of protein stability that phosphorylation causes, it does apparently not affect the unfolding pathway that was previously elucidated for rNP. Consistent with this two-state model, native PAGE clearly shows that only two protein species, pentamers and monomers, are detected during the unfolding transition of eNP (data not shown). Therefore, the unfolding transition in the presence of guanidinium salts or urea fits well to a two-state model, with no intermediates detected either by fluorescence spectroscopy or by native PAGE.

DISCUSSION

The use of several biochemical and biophysical techniques has allowed us to study the conformational stability of nucleoplasmin and the description of its unfolding pathway in the presence of chemical denaturants. The role that the increasing phosphorylation level in natural oocyte and egg nucleoplasmin plays in protein stability has also been characterized. We find that the remarkable stability of nonphosphorylated recombinant NP is required to withstand the destabilization caused by phosphorylation-induced protein activation.

Denaturation of oligomeric, in contrast to monomeric, proteins can involve two different processes, dissociation and unfolding (*23, 24*), in which at least three distinct molecular species might coexist, namely, native oligomer, dissociated monomers, and unfolded polypeptide chains (*25*). There also may be partially unfolded but still intact oligomers (*26*). Often, dissociation and unfolding are structurally coupled, and the processes kinetically overlap. Thus, the oligomer → monomer and monomer → unfolded chain transformations appear experimentally as a two-state transition, oligomer → unfolded monomers (*27*), although a partially (un)folded pentamer might exist in a narrow denaturant concentration range (see below).

Nucleoplasmin structural data indicate that the structure of the monomer is stabilized by a compact hydrophobic core (containing 37 hydrophobic residues), a network of backbone and side chain hydrogen bonds, and salt bridges (*5, 28*). On the other hand, a β-hairpin of each monomer lies approximately perpendicular across strands of an adjacent

monomer forming the interface between them. The residues buried at this interface (that represent approximately 32% of the average surface area of a monomer and constitute part of the hydrophobic core of the monomer) create extensive hydrophobic interactions between adjacent NP monomers, thus interconnecting the hydrophobic cores of adjacent monomers and forming a continuous ring that may provide a major stabilizing force in the formation of NP pentamers. Therefore, intersubunit interfaces within the pentamer are fundamental to maintenance of not only oligomer stability but also a (partially) folded monomer (*5, 29*). This evidence suggests that the NP monomer does not exist independently in solution. Indeed, structured monomers cannot be observed under any of the experimental conditions that were assayed. Monomers isolated by gel filtration display fluorescence properties of the denatured state, indicating that disruption of intersubunit contacts destroys the integrity of an essential protein region that also stabilizes the monomer structure, and therefore, as soon as NP dissociates, the resulting monomers fully unfold. Thermodynamic studies of the structural stability of chaperonin cpn10 from different species have also revealed that their structural integrity was maintained, in large part, by intersubunit interactions (*26, 30, 31*). Furthermore, the important contribution of the hydrophobic core formed by the intersubunit interfaces to pentamer stability might explain the different ability of guanidinium salts and urea to unfold nucleoplasmin. Guanidinium is considerably more effective than urea in disrupting indole−indole interactions, and probably all hydrophobic interactions involving aromatic and aliphatic amino acid side chains (*32*). Consequently, GuHCl and GuSCN denature rNP in a highly cooperative manner with D_{50} values of 5.1 and 1.8, respectively, GuSCN being thus 2.8-fold times more effective as a denaturant than GuHCl, a value significantly close to the factor of 2.3 obtained for other proteins (*33*). The higher efficiency of GuSCN is explained by a higher partition coefficient that facilitates its binding to native proteins (*34*).

NP is considered a partially disordered protein (*35*) due to the noncanonical structure of the tail domain (*7*) and its sensitivity to proteases (*36*). All the algorithms used (*37–39*) to analyze the protein sequence predict with high reliability that the last 80 residues of NP are natively disordered. It is believed that these natively disorder proteins lack a fixed structure and exist as dynamic ensembles of interconverting structures that mediate their signaling or regulatory function, allowing them to bind different ligands and facilitate post-translational modifications (*40*). The NP tail domain could function as a binding domain involved in recognizing different ligands as histones and nuclear transport receptors (*41*), being the target of some of the posttranslational modifications in the natural NP variants (*10*). Since the ensemble of native conformations will be differently destabilized by a chaotropic agent, it is not expected that a fluctuating flexible domain would give rise to a cooperative unfolding process, in contrast to what is experimentally observed for rNPW19F. This unexpected behavior that suggests a fixed rather than a flexible structure might be a consequence of structural coupling of both protein domains, which would result in the stabilization of the tail domain against the chemical challenge. Interdomain interactions could be stabilized by ionic contacts, as suggested by the pentamer expansion observed at high ionic strengths by gel filtration, which might be a consequence of weakening of these interactions. On the other hand, the unfolding behavior of rNPW126F (D_{50} = 1.9 and $\Delta G_{unf,w}$ = 58.8 kcal/mol) indicates that the core domain of NP (where the tryptophan reporter is located) is responsible for the high chemical and thermal stability of this protein, in agreement with previous works (*7, 12*).

During activation of oocytes to eggs, NP undergoes hyperphosphorylation (*9, 10*)which enhances the ability of the protein to remodel chromatin through specific interactions with histones and histone-like proteins (*9, 10*). In this context, we sought to analyze the conformational stability of nucleoplasmin phosphorylated to different levels. Although the secondary structure of natural (phosphorylated to different extents) and recombinant (nonphosphorylated) NP suggests that phosphoryl groups do not significantly modify this structural level (*7*), results shown here clearly demonstrate that they modulate NP stability. This is evidenced by a reduction of both thermal (*12*) and chemical stability against the three denaturants tested. Progressive phosphorylation of oNP and eNP enhances long- and/or short-range electrostatic repulsion, which in turn results in a destabilization of the protein oligomeric structure. Gel filtration of the three NP variants shows that the elution volume decreases as the number of phosphoryl groups increases (*7*), most likely due to a phosphorylation-induced expansion of the structure of oNP and eNP as a consequence of electrostatic repulsions. The comparison of the sedimentation coefficients of rNP and eNP ($s_{w,20}$ = 6.5 and 6.9 S, respectively, obtained under experimental conditions different from ours) (*22*) also indicates a more extended conformation of phosphorylated eNP. In our case, an increased salt concentration diminishes the level of phosphorylation-induced destabilization of eNP, as seen by the upshift of urea D_{50} values and the thermal denaturation temperature (*12*). This could be explained assuming that salts shield the electrostatic repulsion caused by phosphorylation.

The effect of phosphorylation on the stability of different proteins has revealed that this posttranscriptional modification can both stabilize and destabilize protein structures (*42–44*). In this context, recent studies have demonstrated that it is possible to improve protein stability by optimizing surface electrostatic interactions (*45, 46*). Among the factors that might contribute to phosphorylation-induced protein stabilization, formation of a network of hydrogen bonds between phosphoryl groups and nearby positively charged residues has been reported (*42, 43, 47*). In contrast, protein destabilization has been related to the ability of the bulky dianionic phosphoryl group to disrupt the helical conformation of the protein (*48*). In our case, the presence of the phosphoryl moieties on the protein surface probably induces some repulsion effects that would weaken some of the structural factors responsible for the NP pentamer stability, not affecting severely the hydrophobic girdle that sustains the pentamer state. This assumption, in addition to the fact that urea is not a salt and therefore cannot mask destabilizing electrostatic interaction and that urea perturbs mainly the hydrogen bonds that stabilize proteins while guanidinium salts are especially effective in disrupting indole−indole and hydrophobic interactions (*32*), might explain the fact that urea better senses the effect of phosphorylation on protein stability (D_{50} = 8.3 and 3.5 for rNP and eNP, respectively)

as compared to the guanidinium salts (D_{50} = 1.8 and 1.4 for GuSCN and 5.1 and 4.5 for GuHCl) and that urea perceives the steadily increasing phosphorylation level in oNP and eNP. However, we cannot rule out the existence of other denaturant−protein interactions that might contribute to the differences mentioned above.

The gradual phosphorylation of nucleoplasmin (rNP < oNP < eNP), besides modulating the chromatin decondensation activity of NP, steadily destabilizes the protein, as evidenced by decreases of 6 (oNP) and 10 kcal/mol (eNP). Incorporation of at least 15 (oNP) or 40 (eNP) phosphoryl groups per protein pentamer would undoubtedly provoke an electrostatic repulsion that destabilizes the protein particle. If we compare the $\Delta G_{unf,w}$ value of rNP with the calculated and normalized average value for a protein of its size (*49*), or with those of other pentameric proteins (*50*), we can suggest that the remarkably stable nonphosphorylated nucleoplasmin might function as a solid scaffold to withstand the destabilizing effect that phosphorylation-mediated activation induces on this pentameric protein without significantly compromising its stability under physiological conditions.

ACKNOWLEDGMENT

We thank I. Arregi for help with protein purification and Dr. G. Rivas from CIB, CSIC (Madrid, Spain), for ultracentifugation analysis.

REFERENCES

1. Laskey, R. A., Mills, A. D., and Morris, R. N. (1977) Assembly of SV40 chromatin in a cell-free system from *Xenopus* eggs. *Cell 10*, 237–243.
2. Laskey, R. A., Honda, B. M., Mills, A. D., and Finch, J. T. (1978) Nucleosomes are assembled by an acidic protein which binds histones and transfers them to DNA. *Nature 275*, 416–420.
3. Earnshaw, W., Honda, B. M., Thomas, J. O., and Laskey, R. (1980) Assembly of nucleosomes: The reaction involving *X. laevis* nucleoplasmin. *Cell 21*, 373–383.
4. Frehlick, L. J., Eirín-López, J. M., and Ausió, J. (2007) New insights into the nucleophosmin/nucleoplasmin family of nuclear chaperones. *BioEssays 29*, 49–59.
5. Dutta, S., Akey, I. V., Dingwall, C., Hartman, K. L., Laue, T., Nolte, R. T., Head, J. F., and Akey, C. W. (2001) The crystal structure of nucleoplasmin-core: Implications for histone binding and nucleosome assembly. *Mol. Cell 8*, 841–853.
6. Namboodiri, V. M. H., Dutta, S., Akey, I. V., Head, J. F., and Akey, C. W. (2003) The crystal structure of *Drosophila* NLP-core provides insight into pentamer formation and histone binding. *Structure 11*, 175–186.
7. Hierro, A., Arizmendi, J. M., De las Rivas, J., Urbaneja, M. A., Prado, A., and Muga, A. (2001) Structural and functional properties of *Escherichia coli*-derived nucleoplasmin. A comparative study of recombinant and natural proteins. *Eur. J. Biochem. 268*, 1739–1748.
8. Fink, A. L. (2005) Natively unfolded proteins. *Curr. Opin. Struct. Biol. 15*, 35–41.
9. Leno, G. H., Mills, A. D., Philpott, A., and Laskey, R. A. (1996) Hyperphosphorylation of nucleoplasmin facilitates *Xenopus* sperm decondensation at fertilization. *J. Biol. Chem. 271*, 7253–7256.
10. Bañuelos, S., Omaetxebarria, M. J., Ramos, I., Larsen, M. L., Arregi, I., Jensen, O. N., Arizmendi, J. M., Prado, A., and Muga, A. (2007) Phosphorylation of both nucleoplasmin domains is required for activation of its chromatin decondensation activity. *J. Biol. Chem. 282*, 21213–21221.
11. Johnson, L. N., and Lewis, R. J. (2001) Structural basis for control by phosphorylation. *Chem. Rev. 101*, 2209–2242.
12. Hierro, A., Arizmendi, J. M., Bañuelos, S., Prado, A., and Muga, A. (2002) Electrostatic interactions at the C-terminal domain of nucleoplasmin modulate its chromatin decondensation activity. *Biochemistry 41*, 6408–6413.
13. Schuck, P. (2000) Size distribution analysis of macromolecules by sedimentation velocity ultracentrifugation and Lamm equation modeling. *Biophys. J. 78*, 1606–1619.
14. Schuck, P., Perugini, M. A., Gonzales, N. R., Howlett, G. J., and Schubert, D. (2002) Size-distribution analysis of proteins by analytical ultracentrifugation: Strategies and application to model systems. *Biophys. J. 82*, 1096–1111.
15. Minton, A. P. (1994) Conservation of signal: A new algorithm for the elimination of the reference concentration as an independently variable parameter in the analysis of sedimentation equilibrium. In *Modern Analytical Ultracentrifugation* (Schuster, T. M., and Sauer, T. M., Eds.) pp 81−93, Birkhäuser, Boston.
16. Laue, T. M., Shah, B. D., Ridgeway, T. M., and Pelletier, S. L. (1992) Interpretation of analytical sedimentation data for proteins. In *Analytical Ultracentrifugation in Biochemistry and Polymer Science* (Harding, S., Rowe, A., and Horton, J., Eds.) pp 90−125, Royal Society of Chemistry, Cambridge, U.K.
17. Prakash, V., and Timasheff, S. N. (1985) In *Methods in Enzymology* (Hirs, C. H. W., and Timasheff, S. N., Eds.) Vol. 117, Chapter 4, p 53, Academic Press, Orlando, FL.
18. Iwata, K., Hozumi, K., Iihara, A., Nomizu, M., Sakairi, N., and Nishi, N. (1999) Mechanism of salmon sperm decondensation by nucleoplasmin. *Int. J. Biol. Macromol. 26*, 95–101.
19. Burstein, E. A., Vedenkina, N. S., and Ivkova, M. N. (1973) Fluorescence and the location of tryptophan residues in protein molecules. *Photochem. Photobiol. 18*, 263–279.
20. Alston, R. W., Lasagna, M., Grimsley, G. R., Scholtz, J. M., Reinhart, G. D., and Pace, C. N. (2008) Tryptophan Fluorescence Reveals the Presence of Long-Range Interactions in the Denatured State of Ribonuclease Sa. *Biophys. J. 94*, 2288–2296.
21. Park, C., and Marqusee, S. (2004) Analysis of the stability of multimeric proteins by effective ΔG and effectives m-values. *Protein Sci. 13*, 2553–2558.
22. Ramos, I., Prado, A., Finn, R. M., Muga, M., and Ausió, J. (2005) Nucleoplasmin-mediated unfolding of chromatin involves the displacement of linker-associated chromatin proteins. *Biochemistry 44*, 8274–8281.
23. Jaenicke, R., and Lilie, H. (2000) Folding and association of oligomeric and multimeric proteins. *Adv. Protein Chem. 53*, 329–401.
24. Neet, K., and Timm, D. (1994) Conformational stability of dimeric proteins: Quantitative studies by equilibrium denaturation. *Protein Sci. 3*, 2167–2174.
25. Reddy, G. B., Bharadwaj, S., and Surolia, A. (1999) Thermal stability and mode of oligomerization of the tetrameric peanut agglutinin: A differential scanning calorimetry study. *Biochemistry 38*, 4464–4470.
26. Guidry, J. J., Moczygemba, C. K., Steede, N. K., Landry, S., and Wittung-Stafshede, P. (2000) Reversible denaturation of oligomeric human chaperonin 10: Denatured state depends on chemical denaturant. *Protein Sci. 9*, 2109–2117.
27. Panse, V. G., Swaminathan, C. P., Aloor, J. J., Surolia, A., and Varadajan, R. (2000) Unfolding thermodynamics of the tetrameric chaperone, SecB. *Biochemistry 39*, 2362–2369.
28. Dutta, S. (2000) The X-ray crystallographic structure of nucleoplasmin core: A chaperone for histone octamer assembly. Ph.D. Thesis, Boston University, Boston.
29. Arnan, C., Prieto, C., Chiva, M., Salvany, L., Ausió, J., Subirana, J. A., and Saperas, N. (2005) Analysis of the stability and function of nucleoplasmin through cysteine mutants. *Arch. Biochem. Biophys. 437*, 205–214.
30. Guidry, J. J., Shewmaker, F., Maskos, K., Landry, S., and Wittung-Stafshede, P. (2003) Probing the interface in a human co-chaperonin heptamer: Residues disrupting oligomeric unfolded state identified. *BMC Biochem. 4*, 14–27.
31. Sakane, I., Ikeda, M., Matsumoto, C., Higurashi, T., Inoue, K., Hongo, K., Mizobata, T., and Kawata, Y. (2004) Structural stability of oligomeric chaperonin 10: The role of two β-strands at the N and C termini in structural stabilization. *J. Mol. Biol. 344*, 1123–1133.
32. Dempsey, C. E., Piggot, T. J., and Mason, P. E. (2005) Dissecting contributions to the denaturant sensitivities of proteins. *Biochemistry 44*, 775–781.
33. Moczygemba, C., Guidry, J., Jones, K. L., Gomes, C. M., Teixeira, M., and Wittung-Stafshede, P. (2001) High stability of a ferredoxin from the hyperthermophilic archaeon *A. ambivalens*: Involvement of electrostatic interactions and cofactors. *Protein Sci. 10*, 1539–1548.

34. Courtenay, E. S., Capp, M. W., and Record, M. T., Jr. (2001) Thermodynamics of interactions of urea and guanidinium salts with protein surface: Relationship between solute effects on protein processes and changes in water-accessible surface area. *Protein Sci. 10*, 2485–2497.
35. Sickmeier, M., Hamilton, J. A., LeGall, T., Vacic, V., Cortese, M. S., Tantos, A., Szabo, B., Tompa, P., Chen, J., Uversky, V. N., Obradovic, Z., and Dunker, A. K. (2007) DisProt: The Database of Disordered Proteins. *Nucleic Acids Res. 35*, D787−D793.
36. Dingwall, C., Sharnick, S. V., and Laskey, R. A. (1982) A polypeptide domain that specifies migration of nucleoplasmin into the nucleus. *Cell 30*, 449–458.
37. Linding, R., Jensen, L. J., Diella, F., Bork, P., Gibson, T. J., and Russell, R. B. (2003) Protein disorder prediction: Implications for structural proteomics. *Structure 11*, 1453–1459.
38. Dosztanyi, Z., Csizmok, V., Tompa, P., and Simon, I. (2005) IUPred: Web server for the prediction of intrinsically unstructured regions of proteins based on estimated energy content. *Bioinformatics 21*, 3433–3434.
39. Peng, K., Radivojac, P., Vucetic, S., Dunker, A. K., and Obradovic, Z. (2006) Length-dependent prediction of protein intrinsic disorder. *BMC Bioinf. 7*, 208–224.
40. Kriwacki, R. W., Hengst, L., Tennant, L., Reed, S. I., and Wright, P. E. (1996) Structural studies of p21Waf1/Cip1/Sdi1 in the free and Cdk2-bound state: Conformational disorder mediates binding diversity. *Proc. Natl. Acad. Sci. U.S.A. 93*, 11504–11509.
41. Prado, A., Ramos, I., Frehlick, L. J., Muga, A., and Ausió, J. (2004) Nucleoplasmin: A nuclear chaperone. *Biochem. Cell Biol. 82*, 437–445.
42. Bishop, S. M., Ross, J. B. A., and Kohanski, R. A. (1999) Autophosphorylation dependent destabilization of the insulin receptor kinase domain: Tryptophan-1175 reports changes in the catalytic cleft. *Biochemistry 38*, 3079–3089.
43. Nosworthy, N. J., Peterkosfsky, A., Konig, S., Seok, Y. J., Szczepanowski, R. H., and Ginsburg, A. (1998) Phosphorylation destabilizes the amino-terminal domain of enzyme I of the *Escherichia coli* phosphoenolpyruvate:sugar phosphotransferase system. *Biochemistry 37*, 6718–6726.
44. Miranda, F. F., Thórólfsson, M., Teigen, K., Sánchez-Ruiz, J. M., and Martínez, A. (2004) Structural and stability effects of phosphorylation: Localized structural changes in phenylalanine hydroxylase. *Protein Sci. 13*, 1219–1226.
45. Pérez-Jiménez, R., Godoy-Ruiz, S., Ibarra-Molero, B., and Sánchez-Ruiz, J. M. (2005) The effect of charge-introduction mutations on *E. coli* thioredoxin stability. *Biophys. Chem. 115*, 105–107.
46. Strickler, S. S., Gribenko, A. V., Gribenko, A. V., Keiffer, T. R., Tomlinson, J., Reihle, T., Loladze, V. V., and Makhatadze, G. I. (2006) Protein stability and surface electrostatics: A charged relationship. *Biochemistry 45*, 2761–2766.
47. Andrew, C. D., Warwicker, J., Jones, G. R., and Doig, A. J. (2002) Effect of phosphorylation on α helix stability as a function of position. *Biochemistry 41*, 1897–1905.
48. Honnappa, S., Jahnke, W., Seelig, J., and Steinmetz, M. (2006) Control of intrinsically disordered stathmin by multisite phosphorylation. *J. Biol. Chem. 281*, 16078–16083.
49. Sánchez-Ruiz, J. M. (1995) Differential Scanning Calorimetry of Proteins. In *Subcellular Biochemistry Volume 24. Proteins: Structure, Function, and Engineering* (Biswas, B. B., and Roy, S., Eds.) pp 133−176, Plenun Press, New York.
50. Pina, D. G., Gómez, J., Villar, E., Johannes, L., and Shnyrov, V. L. (2003) Thermodynamic Analysis of the Structural Stability of the Shiga Toxin B-Subunit. *Biochemistry 42*, 9498–9506.

BI8002555